

Thermal structure, coupling and metamorphism in the Mexican subduction zone beneath Guerrero

V. C. Manea,¹ M. Manea,¹ V. Kostoglodov,¹ C. A. Currie^{2,3} and G. Sewell⁴

¹Instituto de Geofísica, Universidad Nacional Autónoma de México (UNAM), México. E-mail: vladym@ollin.igeofcu.unam.mx

²School of Earth and Ocean Sciences, University of Victoria, Victoria, BC, Canada

³Pacific Geoscience Centre, Geological Survey of Canada, Sidney, BC, Canada

⁴University of Texas, El Paso, USA

Accepted 2004 April 14. Received 2004 April 12; in original form 2003 January 28

SUMMARY

Temperature is one of the most important factors that controls the extent and location of the seismogenic coupled and transition, partially coupled segments of the subduction interplate fault. The width of the coupled fault inferred from the continuous GPS observations for the steady interseismic period and the transient width of the last slow aseismic slip event ($M_w \sim 7.5$) that occurred in the Guerrero subduction zone in 2001–2002 extends up to 180–220 km from the trench. Previous thermal models do not consider this extremely wide coupled interface in Guerrero subduction zone that is characterized by shallow subhorizontal plate contact. In this study, a finite element model is applied to examine the temperature constraints on the width of the coupled area. The numerical scheme solves a system of 2-D Stokes equation and 2-D steady-state heat transfer equations.

The updip limit of the coupling zone is taken between 100 and 150 °C, while the downdip limit is accepted at 450 °C as the transition from partial coupling to stable sliding. From the entire coupled zone, the seismogenic zone extends only up to ~82 km from the trench (inferred from the rupture width of large subduction thrust earthquakes), corresponding to the 250 °C isotherm. Only a small amount of frictional heating is needed to fit the intersection of the 450 °C isotherm and the subducting plate surface at 180–205 km from the trench.

The calculated geotherms in the subducting slab and the phase diagram for MORB are used to estimate the metamorphic sequences within the oceanic subducting crust. A certain correlation exists between the metamorphic sequences and the variation of the coupling along the interplate fault.

Key words: coupling, flat subduction, Mexican subduction zone, thermal models.

1 INTRODUCTION

The most crucial feature of the Mexican subduction zone is a shallow subhorizontal plate interface in its central part beneath the Guerrero state (Kostoglodov *et al.* 1996). This particular configuration of the young subducting Cocos plate (~14 Ma) apparently creates some distinct geodynamic consequences, such as very thin continental lithosphere, relatively shallow intraslab seismicity, remote position of the volcanic front, etc. The Guerrero seismic gap extending ~120 km northwest from Acapulco (Fig. 1) has not ruptured since 1911, meanwhile the neighbouring zones suffered large subduction thrust earthquakes.

Recent continuous GPS observations in Guerrero show that the interplate coupling during the steady-state interseismic period is abnormally wide, extending up to 180–220 km inland from the trench (Kostoglodov *et al.* 2003). A few thermal models of the subduction zone in Guerrero have been proposed (Currie *et al.* 2002), however

they take no account of the ~200-km-wide coupled zone (because of the lack of this information at that time).

In a recent study of Kostoglodov *et al.* (2003), the surface deformation inferred from GPS measurements during the last slow-slip earthquake are compared with the results from the 2-D forward displacement model for an elastic half-space (Savage 1983). The steady-state component of GPS site velocities is modelled as constant-velocity slip on the subduction interface. In this approach, a virtual slip or back slip with magnitude and direction equal and opposite the relative plate motion is used to represent frictional coupling on the megathrust. On any given discrete segment of the megathrust, it is assumed that the steady-state slip rate is some fraction (coupling (α)) of the relative plate motion: $\alpha = S_b/S_{rpm}$, where $\alpha = [0-1]$; S_b is the back-slip rate; S_{rpm} is the relative slip between the Cocos and North American plates (5.5 cm yr⁻¹ from the NUVEL 1A model of DeMets *et al.* 1994). When $\alpha = 0$, no coupling between the two plates is considered (perfectly decoupled back-slip segment) and

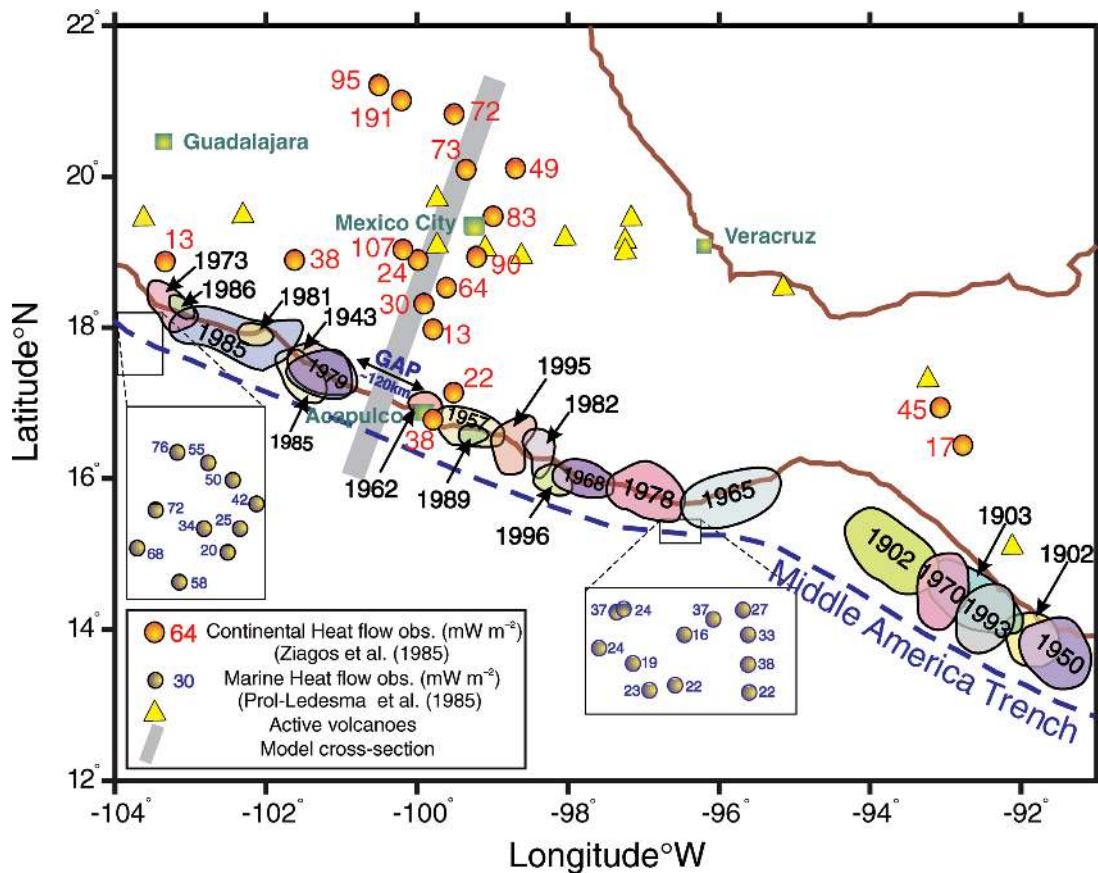


Figure 1. Distribution of the heat flow data and the location of modelled cross-section in Guerrero. Large orange circles are continental heat flow measurements in mW m^{-2} (Ziagos *et al.* 1985). Small light blue circles in the insets are ocean heat flow measurements in mW m^{-2} (Prol-Ledesma *et al.* 1989). Yellow triangles show the location of active volcanoes in Mexico. Green squares are the major cities. Grey thick line is the modelled cross-section. Also, the rupture areas for megathrust earthquakes along the Mexican coast are shown (Kostoglodov & Pacheco 1999). The extension of the seismic gap in Guerrero is ~ 120 km northwest from Acapulco.

$\alpha = 1$ indicates a full coupling between the oceanic plate and the overriding continental plate (perfectly coupled back-slip segment).

Using the slab geometry from Kostoglodov *et al.* (1996) and a wide partially coupled zone (~ 220 km from the trench), the dislocation model of Kostoglodov *et al.* (2003) shows a reasonably good fit with the observations (Fig. 2). The best model fits the GPS measurements when the plate interface is partially locked on three segments. The first segment is located in the shallower part of the subducting plate with a coupling of $\alpha = 0.9$. It follows two partially coupled segments with $\alpha = 0.7$. The rest of the interface slips freely ($\alpha = 0.0$). In order to obtain a good fit with the observed data, the partially coupled segment was extended up to 215 km from trench.

A dislocation model with the slab geometry from Currie *et al.* (2002) does not offer a good fit with the observed surface deformations, because of the slab geometry and the limited extent of the partially coupled zone.

In view of these new results for the Guerrero subduction zone, the motivation of the present paper is to review the previously published thermal structure for Guerrero and to offer a possible explanation for the largest silent earthquake ever recorded. The largest slow aseismic slip event in Guerrero (2001–2002) has developed almost over the entire width of the previously coupled plate interface (Kostoglodov *et al.* 2003). The discovery of this large slow aseismic event and the

non-episodic occurrence of such an extensive slow earthquake in the Guerrero gap (Fig. 1) call for an examination of the controlling factors and physical conditions associated with these events.

It is assumed that pressure, temperature and rock composition provide the key controls on the extent and location of the seismogenic zone (Peacock & Hyndman 1999). The main goal of this study is to analyse this wide subhorizontal coupled plate interface beneath Guerrero using a numerical modelling of the thermal structure in this subduction zone. The interplate geometry and coupling extension is better constrained (Kostoglodov *et al.* 2003) than in the previous models (Currie *et al.* 2002). We developed the 2-D steady-state thermal models using a numerical scheme with a system of 2-D steady-state heat transfer equation and 2-D Stokes equations.

The updip and downdip limits of the interplate and slow-slip earthquakes have been attributed to a certain temperature range. While the seismogenic, coupled zone, where large interplate earthquakes often occur, is confined by 100–150 and ≤ 350 °C isotherms, the partially coupled, transient zone, is delimited by ≤ 350 and 450 °C isotherms (Fig. 3 Wang 1980; Blanpied *et al.* 1995; Tse & Rice 1986; Hyndman & Wang 1993). The position of the updip limit of the seismogenic zone at 100–150 °C has been attributed to the presence of the stable subducted sliding sediments (Vrolijk 1990).

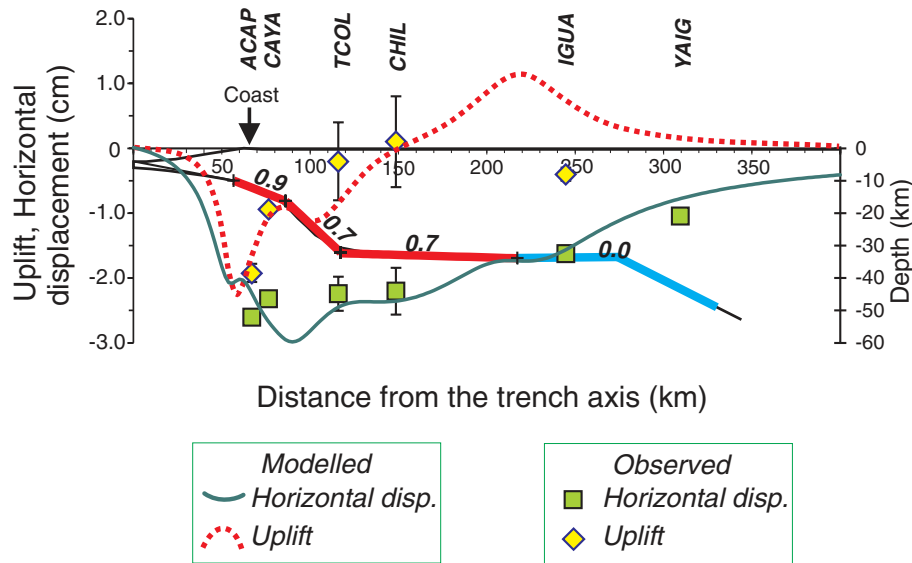


Figure 2. Dislocation model for the interseismic steady-state deformations observed on the GPS stations. The interface is partially locked on three segments (thick lines; bold numbers indicating the fraction of locking). The rest of the interface slips freely. The model fits reasonably well the observed data. Displacement errors bars 1σ are shown. Reproduced from fig. 4 of Kostoglodov *et al.* (2003), copyright by the American Geophysical Union.

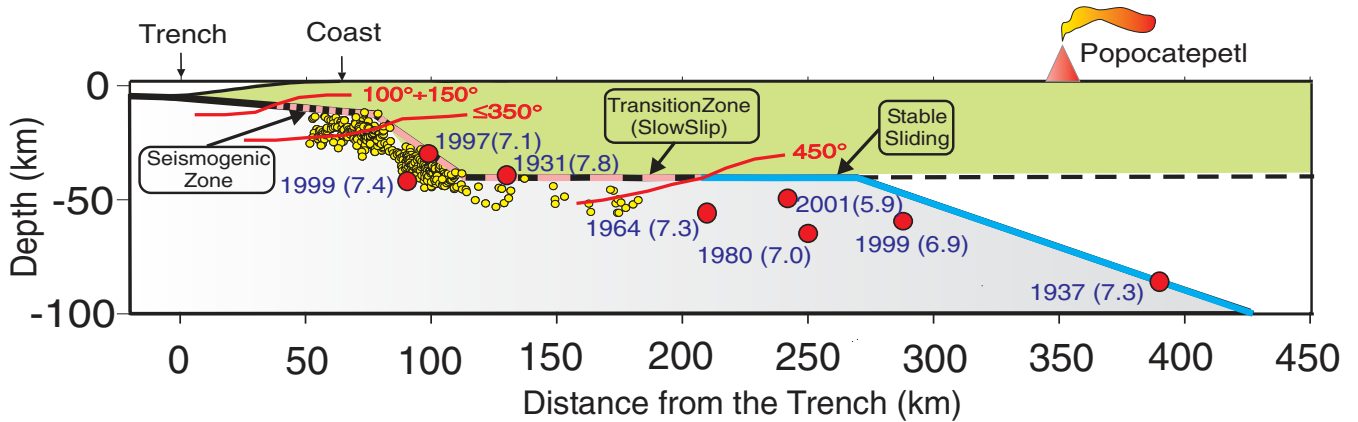


Figure 3. The updip and downdip limits of the seismogenic and slow-slip zones. The seismogenic zone (fine dashed black–pink line) is confined by 100–150 and $\leq 350^\circ\text{C}$ isotherms. The partially coupled zone (coarse dashed black–pink line), where slow earthquakes are proposed to occur, is delimited by $\leq 350^\circ\text{C}$ and 450°C isotherms. Beyond 450°C , the oceanic plate and the overriding plate are considered completely decoupled (continuous light blue line). Small yellow circles represent the background seismic activity with low magnitude ($M_w \leq 4$). The red circles represent intraslab earthquakes with magnitude $M_w \geq 5.9$.

Because laboratory experiments (Blanpied *et al.* 1995) show that continental rocks exhibit a transition from velocity weakening to velocity strengthening at $325\text{--}350^\circ\text{C}$, this temperature range was proposed to be the downdip limit of the seismogenic zone. However, the experiments were carried out on quartzo-feldspathic continental rock type, while the mineralogical composition of the subducting oceanic crust is quite different. Therefore, the $325\text{--}350^\circ\text{C}$ temperature range for the downdip limit of the seismogenic zone should not be considered so restrictive, it may be quite variable from one subduction zone to another.

The final intention of this study is to verify a possible relationship between the predicted metamorphic facies along the subducting oceanic plate (Hacker *et al.* 2003) and the width of the interplate coupling inferred from the modelling of the surface crustal deformations observed during the interseismic steady-state period and the last silent earthquake in Guerrero.

2 MODELLING PROCEDURE

A system of 2-D Stokes equations and the 2-D steady-state heat transfer equation are solved for the Guerrero cross-section (Fig. 1) using the finite element solver PDE2D (<http://pde2d.com/>). The equations in an explicit form are:

$$\begin{cases} \frac{\partial \left(-P + 2\eta \frac{\partial u}{\partial x} \right)}{\partial x} + \frac{\partial \left[\eta \left(\frac{\partial u}{\partial y} + \frac{\partial v}{\partial x} \right) \right]}{\partial y} = 0 \\ \frac{\partial \left[\eta \left(\frac{\partial u}{\partial y} + \frac{\partial v}{\partial x} \right) \right]}{\partial x} + \frac{\partial \left(-P + 2\eta \frac{\partial v}{\partial y} \right)}{\partial y} = -\rho \cdot g \\ C_p \left(u \frac{\partial T}{\partial x} + v \frac{\partial T}{\partial y} \right) = \frac{\partial}{\partial x} \left(k \frac{\partial T}{\partial x} \right) + \frac{\partial}{\partial y} \left(k \frac{\partial T}{\partial y} \right) + Q + Q_{sh}, \end{cases} \quad (1)$$

Table 1. Summary of the thermal parameters used in the models. (Compilation from: Vacquier *et al.* (1967); Smith *et al.* (1979); Ziagos *et al.* (1985); Prol-Ledesma *et al.* (1989); Peacock & Wang (1999)).

Geological unit	Thermal conductivity ($\text{W m}^{-1} \text{K}^{-1}$)			Heat production ($\mu\text{W m}^{-3}$)	Thermal capacity ($\text{MJ m}^{-3} \text{K}^{-1}$)
	Forearc	Volcanic-arc	Backarc		
Oceanic sediments		1.00–2.00*		1.00	2.50
Continental crust (0–15 Km)	2.00	3.00	2.50	0.65	2.50
Continental crust (15–40 Km)	2.00	3.00	2.50	0.20	2.50
Continental mantle		3.10		0.01	3.30
Oceanic lithosphere		2.90		0.02	3.30

*Increase linearly with distance from the deformation front up to a depth of 10 km.

where:

- P is pressure (Pa),
- η is mantle wedge viscosity (isoviscous mantle wedge; Pa s),
- u is the horizontal component of the velocity (m s^{-1}),
- v is the vertical component of the velocity (m s^{-1}),
- ρ is density (kg m^{-3}),
- T is temperature ($^{\circ}\text{C}$),
- C_p is thermal capacity ($\text{MJ m}^{-3}\text{K}^{-1}$),
- k is thermal conductivity ($\text{W m}^{-1}\text{K}^{-1}$),
- Q is radiogenic heat production (W m^{-3}),
- Q_{sh} is volumetric shear heating (W m^{-3}).

Because this paper focuses on the forearc thermal structure, the present thermal models consider only an isoviscous mantle wedge. Models with strong temperature-dependent viscosity and magma transport are presented in detail in a recent paper of Manea *et al.* (2004).

The Stokes equations are solved only for the mantle wedge, while the heat transfer equation is solved for the entire model. The linear system solver used by the present numerical scheme is the frontal method, which represents an out-of-core version of the band solver (uses a reverse Cuthill–McKee ordering). In the present numerical scheme, the penalty method formulation is used, P being replaced by $P = -\alpha' \cdot (\frac{\partial u}{\partial x} + \frac{\partial v}{\partial y})$, where α' is large, on the order of $\frac{\eta}{\sqrt{\epsilon}}$ (ϵ is the machine relative precision). In other words, the material is taken to be almost incompressible, so that a large pressure results in a small decrease in volume, and the continuity equation ($\frac{\partial u}{\partial x} + \frac{\partial v}{\partial y} = 0$) is almost satisfied.

The connection between the Stokes and heat transfer equations is the velocity field. In terms of displacements, the velocity of the oceanic plate is considered with reference to the continental plate. Thus, the convergence rate of 5.5 cm yr^{-1} between the Cocos and North American plates is used in our models (DeMets *et al.* 1994). The velocities in the subducting Cocos slab beneath the volcanic arc are set at 5.5 cm yr^{-1} ; therefore, the interface with the mantle wedge is pre-defined. The boundary between the mantle wedge and overlying lithosphere is considered fixed.

The finite element grids extend from 20 km seaward of the trench up to 600 km landward. The lower limit of the grid follows the shape of the subducting plate upper surface (Kostoglodov *et al.* 1996) at 100 km-depth distance. The thickness of continental crust of 40 km is assumed for the modelling, which is consistent with the values inferred from the seismic refraction surveys and gravity modelling (Valdes *et al.* 1986; Arzate *et al.* 1993).

The modelled profile is subdivided in three regions: forearc, volcanic arc and backarc. The continental crust in every region consists of two layers: the upper crust (15 km thick) and the lower crust (25 km thick). A summary of the thermal parameters used in the mod-

els is presented in Table 1 (compilation from: Vacquier *et al.* 1967; Smith *et al.* 1979; Ziagos *et al.* 1985; Prol-Ledesma *et al.* 1989; Peacock & Wang 1999).

The average radioactive heat production in the upper continental crust reported by Ziagos *et al.* (1985) is approximately $1.3 \pm 0.6 \mu\text{W m}^{-3}$. It has an exponential decrease from the upper crust down to the lower crust. Because the slow slips occurrence is located in the forearc area, we centre the attention to fit the modelled surface forearc heat flow to the observed heat flow data (Fig. 1). Therefore, the radioactive heat production for the upper crust is taken to be $0.7 \mu\text{W m}^{-3}$ (this value is within the 95 per cent confidence interval of the estimate of Ziagos *et al.* (1985)), while a value of $0.2 \mu\text{W m}^{-3}$ is assumed for the lower crust. This reduction has a negligible effect on the thermal structure of the subduction interface.

The upper and lower boundaries of the model are maintained at constant temperatures of 0 and $1450 \text{ }^{\circ}\text{C}$ (asthenosphere), correspondingly. The right (landward) vertical boundary condition (BC) is defined by a $20 \text{ }^{\circ}\text{C km}^{-1}$ thermal gradient for the continental crust. This value is in agreement with the backarc thermal gradient of $17.8\text{--}20.2 \text{ }^{\circ}\text{C km}^{-1}$ reported by Ziagos *et al.* (1985). Although the conductive heat equation with internal heating does not produce a linear temperature increase with depth, the heat flow from the mantle controls the thermal gradient in the crust in the backarc zone. Furthermore, this landward boundary is located far away ($\sim 400 \text{ km}$) from the coupled plate interface and does not produce a significant effect on it (the heat transfer by conduction can be noticeable only to a relatively small distance). Therefore, we simplify this BC by a linear temperature increase with depth. It is considered that the temperature at the Moho beneath arcs and backarcs is above $800 \text{ }^{\circ}\text{C}$ (Bostock *et al.* 2002) and $1450 \text{ }^{\circ}\text{C}$ at 100 km depth in the asthenosphere. In our models, we consider the Moho temperature in the backarc to be $850 \text{ }^{\circ}\text{C}$ and a linear thermal gradient for the continental crust of $20 \text{ }^{\circ}\text{C km}^{-1}$. Given that in our models the Moho is located at 40 km depth, the mantle wedge right BC is represented by a $10 \text{ }^{\circ}\text{C km}^{-1}$ thermal gradient down to the depth of 100 km. Underneath 100 km depth, no horizontal conductive heat flow is specified. Beneath the Moho, for the right boundary corresponding to the mantle wedge, the BCs are:

$$\begin{cases} (-P + 2 \cdot \eta \cdot \frac{\partial u}{\partial x}) \cdot \vec{n}_x + \eta \cdot (\frac{\partial u}{\partial y} + \frac{\partial v}{\partial x}) \cdot \vec{n}_y = GB1, \\ \eta \cdot (\frac{\partial u}{\partial y} + \frac{\partial v}{\partial x}) \cdot \vec{n}_x + (-P + 2 \cdot \eta \cdot \frac{\partial v}{\partial y}) \cdot \vec{n}_y = GB2, \end{cases}$$

which are obtained by balancing the internal (stress induced) forces against the external boundary forces, called tractions ($GB1$ and $GB2$). Therefore, beneath the Moho, where there is no external force applied, $GB1 = GB2 = 0$. Because the slab is considered as a rigid

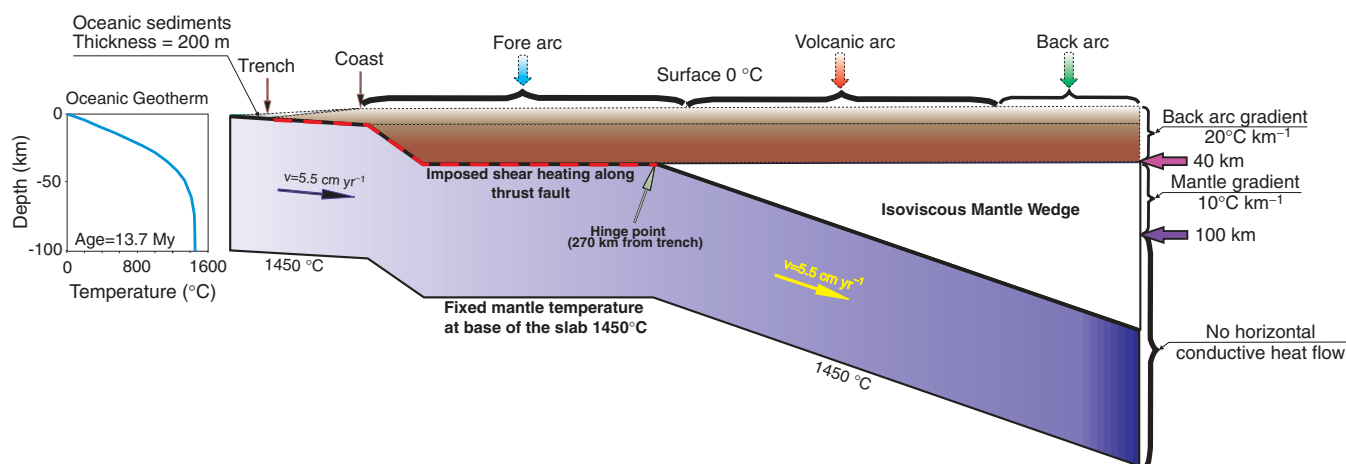


Figure 4. Boundary condition (BC) and thermal parameters used in the modelling. The upper and lower boundaries are maintained at the constant temperatures of 0 and $1450 \text{ }^\circ\text{C}$ (asthenosphere), correspondingly. The right (landward) vertical BC is defined by the $20 \text{ }^\circ\text{C km}^{-1}$ thermal gradient in the continental crust and $10 \text{ }^\circ\text{C km}^{-1}$ up to a depth of 100 km. Deeper, no horizontal conductive heat flow is specified. The left (seaward) BC (shown in the inset) is the 1-D geotherm for the oceanic plate. The oceanic geotherm is corrected for the time-dependent sedimentation history (Wang & Davis 1992), assuming a constant porosity–depth profile of the sediment column and a uniform sediment thickness of 200 m at the trench. The oceanic plate is subducting at a constant rate of 5.5 cm yr^{-1} , while the continental crust is considered fixed. The modelled profile is subdivided into three regions: forearc, volcanic arc and backarc. In each region, the continental crust consists of two layers: the upper crust and the lower crust. A summary of the thermal parameters used in the models is presented in Table 1.

body, for the deepest part of the right boundary, the velocity of the subducting slab is used. The left (seaward) BC is a 1-D geotherm for the oceanic plate. This geotherm is calculated by allowing a conductive cooling of the zero age half-space during the time equal to the age of the oceanic plate at the trench. This geotherm is corrected for the time-dependent sedimentation history (Wang & Davis 1992), assuming a constant porosity–depth profile of the sediment column and a uniform sediment thickness of 200 m (Moore *et al.* 1982) at the trench. The calculated oceanic geotherm is shown in Fig. 4.

The plate age at the trench is of 13.7 Myr according to the interpretation of Pacific–Cocos seafloor spreading magnetic anomaly lineations by Klitgord & Mammerrickx (1982). The plate interface geometry is constrained by the local seismicity and the gravity anomalies modelling (Kostoglodov *et al.* 1996). The Cocos slab has an initial dip of $<15^\circ$, which steepens to as much as 35° near the coast and subsequently becomes subhorizontal beneath the overriding continental lithosphere. At 270 km from the trench, the slab dips into the asthenosphere at 20° (Fig. 3). The two dense clusters of seismic events beneath the coast (small yellow circles in Fig. 3), representing the background seismic activity with low magnitude ($M_w \leq 4$), appear to be related to the sharp bending–unbending of the plate in this region at ~ 80 and ~ 115 km from the trench. Important stress concentrations and pressure variations (up to some 100 MPa) along the thrust fault are likely to appear in this region.

Marine heat flow measurements at the Middle American trench (Prol–Ledesma *et al.* 1989) revealed anomalously low (Fig. 1) average values of $\sim 30 \text{ mW m}^{-2}$, suggesting that the hydrothermal circulation might be active in the upper part of the oceanic crust near the trench. Unfortunately, the maximum depth as well as the extension of the hydrothermal circulation layer is unknown. Given all these uncertainties, our models do not include the cooling of the oceanic plate at the trench as result of hydrothermal circulation. However, the effect of the hydrothermal circulation becomes insignificant at distances greater than ~ 100 km from the trench. The hydrothermal circulation shifts the position of the 100 – $150 \text{ }^\circ\text{C}$ isotherms with less than 10 km landward (Currie *et al.* 2002), therefore introducing only a relatively small error in the estimate of the upper limit of the seismogenic zone.

The long-term continuous sliding between the subducting and the continental plates along the thrust fault should produce frictional heating. We introduced in the models a small degree of frictional heating using the Byerlee’s friction law (Byerlee 1978). Frictional heating is limited to a maximum depth of 40 km, which corresponds to the contact between the oceanic plate and the mantle wedge. The Pore Pressure Ratio, PPR (the ratio between the hydrostatic and lithostatic pressures; $\text{PPR} \leq 1$, $\text{PPR} = 1$, means no frictional heating), is set in order to fit the extent of the coupled zone ($450 \text{ }^\circ\text{C}$ isotherm) at 180 and 205 km from the trench.

The uncertainties in the forearc thermal models arise mainly from errors in the thermal constants of the continental crust and the oceanic lithosphere and plate geometry. Underneath the volcanic arc, the major uncertainties come from the thermal structure of the mantle wedge. Recent thermal models for the Central Mexican Volcanic Belt (Manea *et al.* 2004), with strong temperature-dependent viscosity, show an increasing with the temperature $<200 \text{ }^\circ\text{C}$ along the slab–wedge interface. A test with reasonably varied parameters show uncertainties in the thermal models of ± 50 – $100 \text{ }^\circ\text{C}$, with the lower limit for the forearc and the higher limit for the volcanic arc.

3 MODELLING RESULTS

The main constraint on the thermal models is the observed surface heat flow (Fig. 1). The heat flow data show a steep increase in front of the Mexican volcanic arc that is common for the subduction zones. In our model, the forearc and the volcanic belt have a surface heat flow of 28 – 35 and $\sim 60 \text{ mW m}^{-2}$, respectively. The forearc heat flow data, 13 – 38 mW m^{-2} , are slightly lower than those predicted by the thermal models, whilst for the volcanic arc the measured values are higher, 64 – 90 mW m^{-2} , than the modelled values. The low modelled heat flow in the forearc region of 28 – 35 mW m^{-2} is a consequence of the heat consumption from the overriding plate by the underlying cold subducting oceanic plate. Our models do not consider magma generation and transport, or temperature-dependent

viscosity in mantle wedge; therefore, the modelled surface heat flow beneath the volcanic arc is smaller than the observed values. The present study focuses only on the forearc zone, the thermal structure beneath the volcanic arc does not influence significantly the thrust fault region (Manea *et al.* 2004). A recent paper of Manea *et al.* (2004), shows a better fit of the surface heat flow in the volcanic arc, as a result of the introduction of a strong temperature-dependence of the asthenospheric viscosity in the mantle wedge. Rayleigh–Taylor instabilities may arise at the slab–wedge interface as a consequence of hydration and partial melting, and compositionally positive buoyant diapirs start to rise toward the base of the continental lithosphere changing the thermal distribution and flow pattern in mantle wedge (Gerya & Yuen 2003). All these effects are not included in the modelling here.

The examples of thermal models, which correspond to the main restrictions (e.g. location and extension of the coupled zones, local seismicity and the hypocentre location of the intraslab earthquakes, etc.) are shown in Fig. 5. The model with PPR = 0.97 is in good agreement with a coupled zone extent up to 180 km from the trench, while the model with PPR = 0.98 better explains the coupled zone extent up to 220 km. The average shear stress along the thrust fault is 13 MPa or an effective coefficient of friction of 0.017 (Wang *et al.* 1995). A smaller value of PPR (<0.97) would increase the amount of frictional heating along the thrust fault, and the position of the 450 °C isotherm moves toward the trench. A greater value of PPR (>0.98) would decrease the frictional heating and, therefore, widen the coupling zone to distances superior to 205 km from the trench. Both thermal models are in agreement with the hypocentre location of the intraslab earthquakes (note that the hypocentral depth estimates of the intraplate earthquakes could have errors up to 20 km). The models indicate that the seismogenic fault (limited by 150 and 250 °C isotherms) in the Guerrero subduction zone is in good agreement with the rupture width of large megathrust earthquakes (Fig. 1) inferred from the aftershock sequences and the models of seismic rupture (Ortiz *et al.* 2000). The position of the 450 °C isotherm can account for the maximum extent of the coupled interplate zone in Guerrero. The slow aseismic slip events are usually occurring on the transient partially coupled plate interface limited by the 250 and 450 °C isotherms.

4 METAMORPHIC FACIES IN THE SUBDUCTING SLAB

Interplate coupling in the subduction zone should depend not only on the P–T conditions but also on the properties of the rock material at the plate contact. In our models, the pressure is considered hydrostatic, although the non-hydrostatic stresses and pressures in subduction zones can reach several 100 MPa along the slab surface. The relationship between the metamorphic facies (Hacker *et al.* 2003) and the coupling degree along the subducting oceanic plate can be revealed using the results of our thermal modelling.

The calculated geotherms of the slab (P–T paths) are plotted on the phase diagrams for MORB and for harzburgite (Hacker *et al.* 2003), in order to determine the metamorphic sequences within the oceanic subducting slab for our two models (Fig. 6). The eclogite facies is bounded by lawsonite-blueschist at low temperatures and by garnet-amphibolite and garnet-granulite facies at high temperatures. The main metamorphic facies in the Guerrero subduction zone are shown in Fig. 7. The crustal material of the subducting Cocos plate passes through zeolite, prehnite-pumpellyite-actinolite facies when $T < 250$ °C, then it enters into lawsonite-blueschist-

jaedite and epidote-blueschist facies at $T < 450$ °C. The position of the hinge point (270 km from the trench) is in good agreement with the transition to the eclogitic facies.

The maximum depth of the intraslab earthquakes in Guerrero (~80 km) correlates with the depth of the stable hydrous phases suggesting that the occurrence of these earthquakes might be related to the dehydration process in the oceanic slab.

The change of metamorphic sequences along the plate interface on the Guerrero profile is consistent with the location and the extension of the coupled zones (Fig. 8). The shallow seismogenic zone with $\alpha = 0.9$, corresponds to the metamorphic facies of zeolite, prehnite-pumpellyite-actinolite, the intermediate partially coupled zone with $\alpha = 0.7$ corresponds to the metamorphic facies of lawsonite-blueschist, while the deeper zone with $\alpha = 0.0$ corresponds to the metamorphic facies of jadeite-lawsonite-blueschist. The blueschist and associated facies (jadeite and lawsonite) in the range of temperature between 250 and 450 °C, and the pressure range of 0.6–1.3 GPa, tends to some ductility. The slow transient slip events seem to be related to the properties of the blueschist facies.

The estimated variation of wt per cent H₂O content with depth along the subducting plate is presented in Fig. 7 (inset). Four to five wt per cent H₂O may be released from the hydrous phases in the subducting slab through a process of dehydration at the depths between 20 and 80 km. Very low shear wave velocities in the cold forearc mantle have been discovered in the southern Cascadia subduction zone (Bostock *et al.* 2002). This is evidence of a highly hydrated and serpentinized material in the forearc region. The same conditions should be expected in the Guerrero subduction zone, too. The presence of serpentine in the mantle wedge can be examined using the phase diagram for harzburgite (Hacker *et al.* 2003). The calculated geotherms plotted in the phase diagram for harzburgite show that the serpentine facies might exist in the mantle wedge (Fig. 6b). The location of the serpentinized mantle wedge tip is critical because it may control the down-dip coupling and slow-slip limits.

5 DISCUSSION AND CONCLUSIONS

The numerical models of temperature distribution in the forearc for the central part of the Guerrero subduction zone are constrained by: the surface heat flow data, the shape of the plate interface estimated from gravity modelling (Kostoglodov *et al.* 1996), seismicity data and recently estimated extension of the coupled interplate fault. The modelled seismogenic zone delimited by 100–150 and 250 °C is in good agreement with the rupture width of large subduction thrust earthquakes in Guerrero. A small degree of frictional heating is required in order to adjust the downdip extension of the partially coupled zone (450 °C isotherm) in accordance with the coupled zone width assessed from the deformation models. The flat subhorizontal plate interface at the distance between 115 and 270 km from the trench is essential in the model to fit the position of the 450 °C isotherm at ~200 km distance from trench corresponding to the maximum extent of the plate coupling.

The change of the metamorphic sequences in the subducting crust apparently relates to the variation of the coupling along the interplate fault, estimated from the observations of surface deformation during the interseismic period (Fig. 8). In the temperature range of 250–450 °C and the pressure of 0.6–1.3 GPa, the metamorphic facies are represented by jadeite-lawsonite-blueschist and epidote-blueschist. The blueschist and associated facies in this temperature and pressure range probably exposes a ductile behaviour,

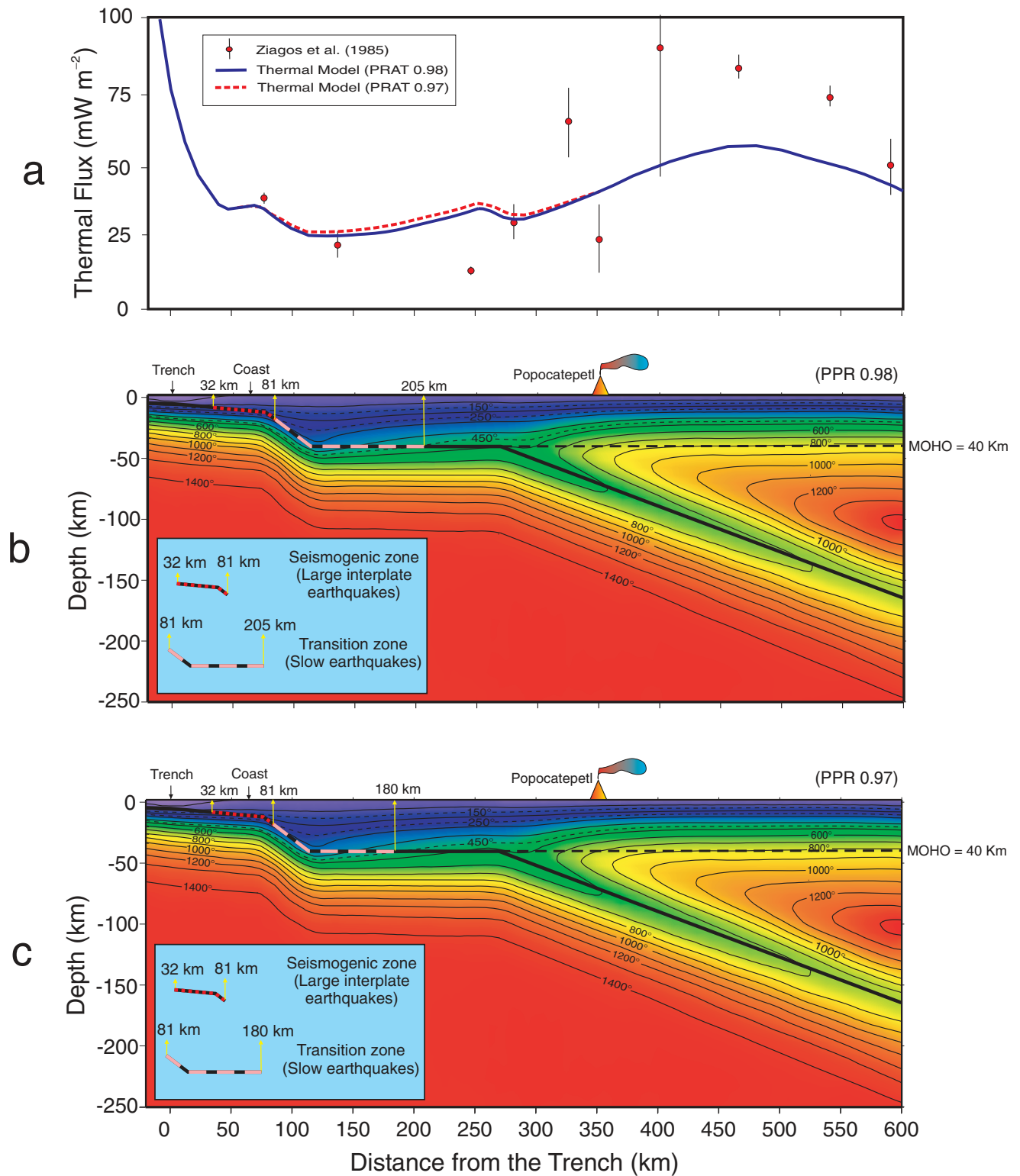


Figure 5. (a) Variations of the surface heat flow along the Guerrero profile. Red dots with vertical error bars are the heat flow measurements from Ziagos *et al.* (1985). Blue solid line is the surface heat flow for the model without frictional heating. Red dashed line corresponds to the model with PPR = 0.97 and the blue solid line to the model with PPR = 0.97. PPR is the pore pressure ratio. (b) The model of steady-state thermal structures for the 13.7 Myr oceanic lithosphere subducting at 5.5 cm yr⁻¹ beneath Guerrero. Frictional heating (PPR = 0.98) is introduced down to a maximum depth of 40 km. The shear stress along the fault is given by Byerlee’s friction law (Byerlee 1978). Orange triangle is the Popocatepetl volcano. Black dashed line is the Moho (40 km depth). The continuous black line indicates the top of the subducting oceanic slab. Short-dashed red segments delimit the seismogenic zone (between 100–150 and 250 °C). Long-dashed pink segment (250–450 °C) shows the zone of partial coupling. The seismogenic zone is located between 32 and 81 km from the trench. The coupling zone extends up to 205 km from the trench. (c) Same as (b) with the frictional heating, PPR = 0.97. The seismogenic zone is between 32 and 81 km. The coupling zone extends up to 180 km from the trench.

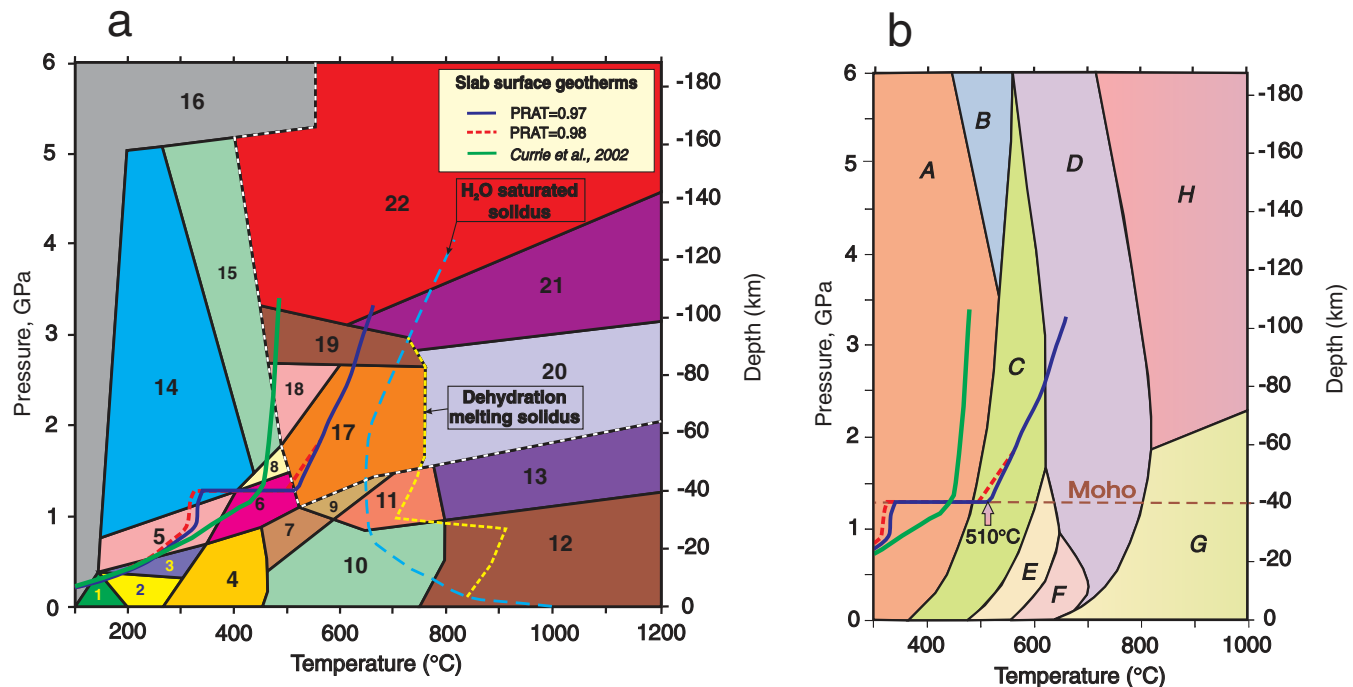


Figure 6. (a) Phase diagram for MORB and maximum H₂O contents (Hacker *et al.* 2003). Calculated geotherms: continuous blue line and dashed red line are P–T paths for the top of the subducting oceanic crust for PPR = 0.97 and 0.98, respectively; continuous green line is the P–T path for the top of the subducting oceanic slab from Currie *et al.* (2002). 1 — Zeolite (4.6 wt per cent H₂O), 2 — prehnite-pumpellyite (4.5 wt per cent H₂O), 3 — pumpellyite-actinolite (4.4 wt per cent H₂O), 4 — greenschist (3.3 wt per cent H₂O), 5 — lawsonite-blueschist (5.4 wt per cent H₂O), 6 — epidote-blueschist (3.1 wt per cent H₂O), 7 — epidote-amphibolite (2.1 wt per cent H₂O), 8 — jadeite-epidote-blueschist (3.1 wt per cent H₂O), 9 — eclogite-amphibole (2.4 wt per cent H₂O), 10 — amphibolite (1.3 wt per cent H₂O), 11 — garnet-amphibolite (1.2 wt per cent H₂O), 12 — granulite (0.5 wt per cent H₂O), 13 — garnet-granulite (0.0 wt per cent H₂O), 14 — jadeite-lawsonite-blueschist (5.4 wt per cent H₂O), 15 — lawsonite-amphibole-eclogite (3.0 wt per cent H₂O), 16 — jadeite-lawsonite-talc-schist (20 wt per cent H₂O), 17 — zoisite-amphibole-eclogite (0.7 wt per cent H₂O), 18 — amphibole-eclogite (0.6 wt per cent H₂O), 19 — zoisite-eclogite (0.3 wt per cent H₂O), 20 — eclogite (0.1 wt per cent H₂O), 21 — coesite-eclogite (0.1 wt per cent H₂O), 22 — diamond-eclogite (0.1 wt per cent H₂O). (b) Phase diagram for harzburgite and maximum H₂O contents (Hacker *et al.* 2003). A — serpentine-chlorite-brucite (14.6 wt per cent H₂O), B — serpentine-chlorite-phase A (12 wt per cent H₂O), C — serpentine-chlorite-dunite (6.2 wt per cent H₂O), D — chlorite-harzburgite (1.4 wt per cent H₂O), E — talc-chlorite-dunite (1.7 wt per cent H₂O), F — anthophyllite-chlorite-dunite (1.7 wt per cent H₂O), G — spinel-harzburgite (0.0 wt per cent H₂O), H — garnet-harzburgite (0.0 wt per cent H₂O). Calculated geotherms are the same as in (a). The calculated geotherms plotted on the phase diagram for harzburgite show that in both of our models the serpentine might exist in the mantle wedge.

which is responsible for the long-term partial coupling and the sporadic aseismic transient slip events. For temperatures superior of 200–300 °C the pre-existing rock undergoes pronounced changes in texture and mineralogy. Pressure and heat are the main agents of metamorphism, the effect of the heat on a pre-existing rock (basalt in our case) being the increased ductility and change in mineral assemblage. Foliated metamorphic rocks, like blueschist, present a layered texture, favouring the ductile behaviour along the slab-overriding plate interface. Ductile deformation resulting from non-hydrostatic stress, which is characteristic for subduction zones, is responsible for the development of imposed anisotropic fabrics in a metamorphic rock like blueschist.

The slab surface geotherm of Currie *et al.* (2002) (Fig. 6) shows a different path. Although the metamorphic facies along the slab surface are basically the same, for depths greater than ~20 km the P–T limits between adjacent facies are different. At ~250 °C, the slab surface geotherm enters in lawsonite-blueschist, then between ~370 and ~450 °C the epidote-blueschist facies is present. The jadeite-lawsonite-blueschist and zoisite-amphibole-eclogite are absent in the Currie *et al.* (2002) thermal model for Guerrero; instead jadeite-epidote-blueschist, lawsonite-amphibole-eclogite and amphibole-eclogite are present. Our models show a good correlation between the position of the hinge point (270 km from the trench)

and the occurrence of the eclogitic facies in the subducted oceanic crust (Fig. 7). The thermal models of Currie *et al.* (2002), illustrate the initiation of the eclogitic facies at a greater depth of ~80 km, although the bending of the slab into the asthenosphere begins at ~50 km depth.

The downdip limit of the seismogenic zone proposed by Currie *et al.* (2002) extends up to 350 °C. From the thermal models of Currie *et al.* (2002) and the phase diagram for MORB, between 250 and 350 °C lawsonite-blueschist facies is present. This temperature range represents half of the total width of the seismogenic zone. If blueschist and associated facies are responsible for the occurrence of the slow earthquakes in Guerrero, then they should not be present in the seismogenic zone. In our models, 250 °C is in good agreement with the maximum extent of the seismogenic zone (~82 km from the trench) and with the onset of the blueschist and associated facies.

Because the model of Currie *et al.* (2002) is colder than our models, the serpentine is not present in the tip of the mantle wedge (Fig. 6b). The proposed alternative for the downdip extension of the thrust zone by the presence of the serpentinized forearc mantle wedge is not supported by the thermal model for Guerrero of Currie *et al.* (2002). Alternatively, the thermal models proposed by this study reveal the presence of a significant amount of serpentine in

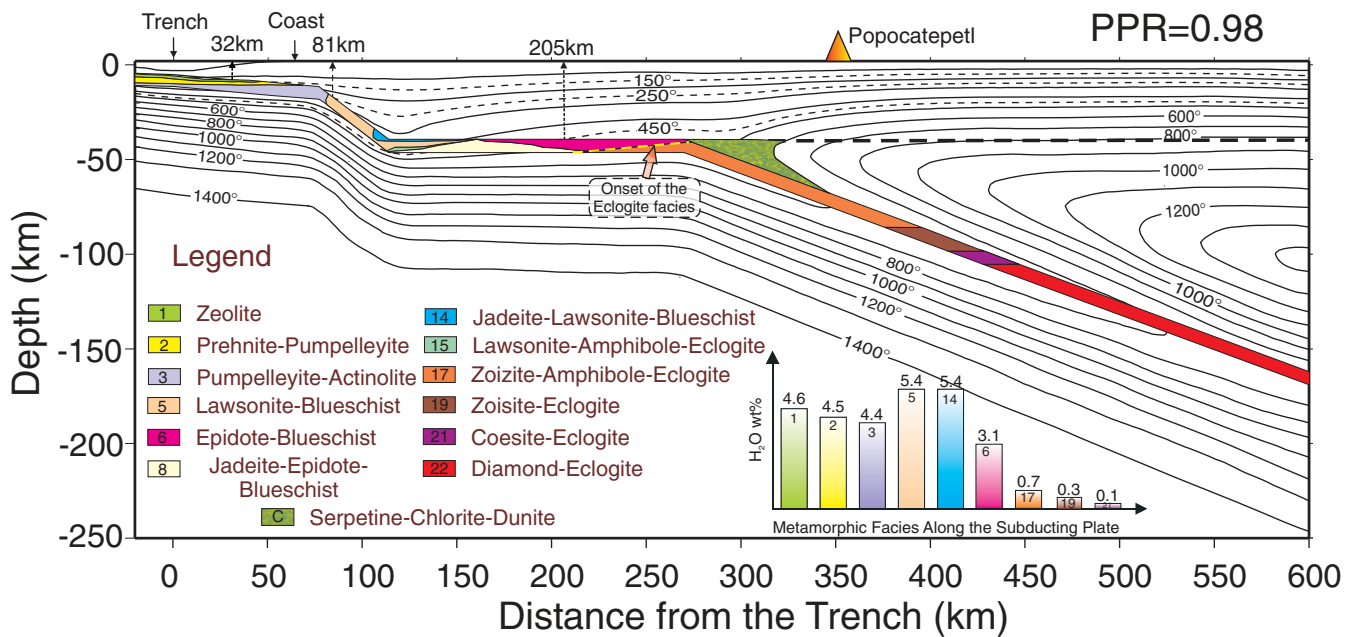


Figure 7. Metamorphic facies along the oceanic subducting crust. The metamorphic facies in the subducting Cocos plate pass through zeolite, prehnite-pumpellyite-actinolite at $T \leq 250^\circ\text{C}$, then lawsonite-blueschist-jaedite and epidote-blueschist at $T \leq 450^\circ\text{C}$. It can be seen from the histogram (inset) wt per cent H_2O versus the metamorphic sequences along the subducting plate that 4–5 wt per cent H_2O may be released from the hydrous phases in the subducting slab through the process of dehydration. The presence of the serpentine in the mantle wedge is predicted from the phase diagram for harzburgite (Fig. 6b; Hacker *et al.* 2003). The dashed yellow line represents the onset of the eclogitic facies in the subducted oceanic crust.

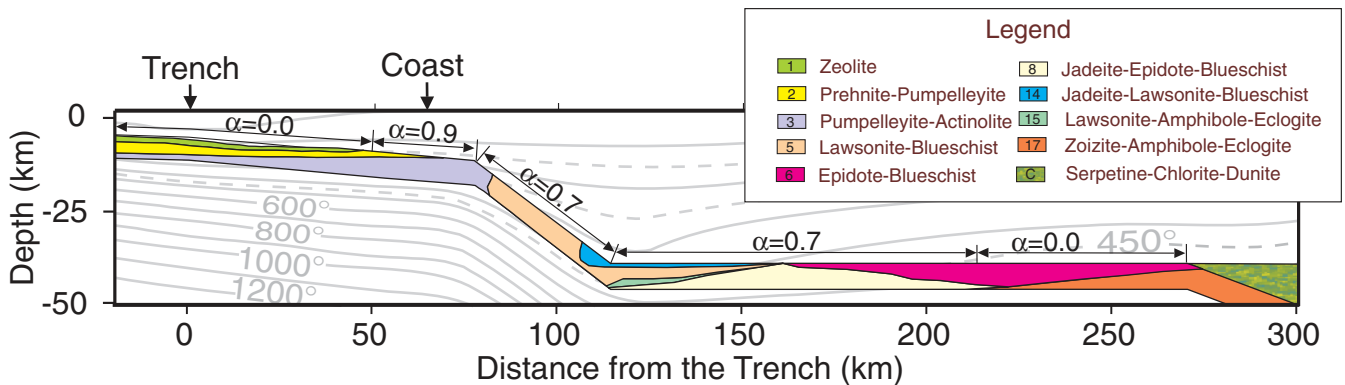


Figure 8. Metamorphic facies along the oceanic subducting crust in the forearc. Superimposed are the coupled segments from the best-fitting dislocation model (Fig. 2). The changes of the metamorphic sequences along the plate interface on Guerrero profile are consistent with the estimates of the location and the extension of the coupled zone.

the tip of the mantle wedge (Figs 6b and 7), sustaining the alternative for the downdip extension of the thrust zone.

According to the phase diagrams for MORB, intensive dehydration in the subducting oceanic crust should occur (Fig. 7 inset) at $T = 250\text{--}450^\circ\text{C}$ and $P = 0.6\text{--}1.3\text{ GPa}$, more than 2 wt per cent H_2O being released during this phase transformation. The occurrence of the slow transient slip events may be related to this dehydration.

ACKNOWLEDGMENTS

The authors are grateful to Harro Schmeling, Steven Ward and an anonymous reviewer for valuable suggestions that greatly improved the manuscript. This study was supported by G25842-T and 37293-T CONACYT grants.

REFERENCES

Arzate, J.A., Mareschal, M. & Urrutia-Fucugauchi, J., 1993. A preliminary crustal model of the Oaxaca continental margin and subduction zone from magnetotelluric and gravity measurements, *Geofis. Int.*, **32**, 441–45.

Blanpied, M.L., Lockner, D.A. & Byerlee, J.D., 1995. Frictional slip of granite at hydrothermal conditions, *J. geophys. Res.*, **100**, 13 045–13 064.

Bostock, M.G., Hyndman, R.D., Rondenay, S. & Peacock, S.M., 2002. An inverted continental Moho and serpentinization of the forearc mantle., *Nature*, **417**, 536–538.

Byerlee, J.D., 1978. Friction of rocks, *Pure appl. Geophys.*, **116**, 615–626.

Currie, C.A., Hyndman, R.D., Wang, K. & Kostoglodov, V., 2002. Thermal models of the Mexico subduction zone: Implications for the megathrust seismic zone, *J. geophys. Res.*, **107**(B12), 2370, doi: 10.1029/2001JB000886.

- DeMets, C., Gordon, R., Argus, D. & Stein, S., 1994. Effect of recent revisions to the geomagnetic reversal time scale on estimates of current plate motions, *Geophys. Res. Lett.*, **21**, 2191–2194.
- Gerya, T.V. & Yuen, D.A., 2003. Rayleigh-Taylor instabilities from hydration and melting propel ‘cold plumes’ at subduction zones, *Earth planet. Sci. Lett.*, **212**, 47–62.
- Hacker, B.R., Abers, G.A. & Peacock, S.M., 2003. Subduction Factory 1. Theoretical mineralogy, densities, seismic wave speeds, and H₂O contents, *J. geophys. Res.*, **108**, doi: 10.1029/2001JB001127.
- Hyndman, R.D. & Wang, K., 1993. Thermal constraints on the zone of major thrust earthquake failure: The Cascadia subduction zone, *J. geophys. Res.*, **98**, 2039–2060.
- Klitgord, K. & Mammerickx, J., 1982. Northern East Pacific Rise: Magnetic anomaly and bathymetric framework, *J. geophys. Res.*, **87**, 6725–6750.
- Kostoglodov, V., Bandy, W., Cominguez, J. & Mena, M., 1996. Gravity and seismicity over the Guerrero seismic gap, Mexico, *Geophys. Res. Lett.*, **23**, 3385–3388.
- Kostoglodov, V. & Pacheco, J. F., 1999. One hundred years of seismicity in Mexico, Inst. de Geofísica., Universidad Nacional Autónoma de México (UNAM), Mexico City.
- Kostoglodov, V., Singh, S.K., Santiago, J.A., Franco, S.I., Larson, K.M., Lowry, A.R. & Bilham, R., 2003. A large silent earthquake in the Guerrero seismic gap, Mexico., *Geophys. Res. Lett.*, **30**(15), 1807, doi: 10.1029/2003GL017219.
- Manea, V.C., Manea, M., Kostoglodov, V., & Sewell, G., 2004. Thermo-mechanical model of the mantle wedge in Central Mexican subduction zone and a blob tracing approach for the magma transport, *Physics of the Earth and Planetary Interiors*, in revision.
- Moore, J.C., Watkins, J.S., Shipley, T.H., McMillen, K.J., Bachman, S.B. & Lundberg, N., 1982. Geology and tectonic evolution of a juvenile accretionary terrane along a truncated convergent margin: Synthesis of results from Leg 66 of the Deep Sea Drilling Project, southern Mexico, *Bull. geol. Soc. Am.*, **93**, 847–861.
- Ortiz, M., Singh, S.K., Kostoglodov, V. & Pacheco, J., 2000. Source areas of the Acapulco-San Marcos, Mexico earthquakes of 1962 (M 7.1; 7.0) and 1957 (M 7.7), as constrained by tsunami and uplift records, *Geofis. Int.*, **39**, 337–348.
- Peacock, S.M. & Hyndman, R.D., 1999. Hydrous minerals in the mantle wedge and the maximum depth of subduction thrust earthquakes, *Geophys. Res. Lett.*, **26**, 2517–2520.
- Peacock, S.M. & Wang, K., 1999. Seismic consequences of warm versus cool subduction metamorphism: Examples from southwest and northeast Japan, *Science*, **286**, 937–939.
- Prol-Ledesma, R.M. et al., 1989. Heat flow variations along the Middle America Trench, *Mar. Geophys. Res.*, **11**, 69–76.
- Savage, J.C., 1983. A dislocation model of strain accumulation and release at a subduction zone, *J. geophys. Res.*, **88**, 4984–4996.
- Smith, D.L., Nuckels, C.E., Jones, R.L. & Cook, G.A., 1979. Distribution of heat flow and radioactive heat generation in northern Mexico, *J. geophys. Res.*, **84**, 2371–2379.
- Tse, S.T. & Rice, J.R., 1986. Crustal earthquake instability in relation to the depth variation of frictional slip properties, *J. geophys. Res.*, **91**, 9452–9472.
- Vacquier, V., Sclater, J.G. & Corry, C.E., 1967. Studies of the thermal state of Earth. The 21st paper: Heat-flow, eastern Pacific, *Bull. Earthq. Res. Inst.*, **45**, 375–393.
- Valdes, C.M. et al., 1986. Crustal structure of Oaxaca, Mexico, from seismic refraction measurements, *Bull. seis. Soc. Am.*, **76**, 547–563.
- Vrolijk, P., 1990. On the mechanical role of smectite in subduction zones, *Geology*, **18**, 703–707.
- Wang, C. Y., 1980. Sediment subduction and frictional sliding in a subduction zone, *Geology*, **8**, 530–533.
- Wang, K. & Davis, E.E., 1992. Thermal effect of marine sedimentation in hydrothermally active areas, *Geophys. J. Int.*, **110**, 70–78.
- Wang, K., Hyndman, R.D. & Yamano, M., 1995. Thermal regime of the southwest Japan subduction zone: Effects of age history of the subducting plate, *Tectonophysics*, **248**, 53–69.
- Ziagos, J.P., Blackwell, D.D. & Mooser, F., 1985. Heat flow in southern Mexico and the thermal effects of subduction, *J. geophys. Res.*, **90**, 5410–5420.